THE SUPERNOVA REMNANT CTA 1

The Paper appended here summarizes the work completed on this project during the referenced period.

NASA Grant NAG5-1938

Final Report

For the Period 15 March 1992 through 14 September 1996

Principal Investigator
Dr. Frederick D. Seward

September 1996

Prepared for:

National Aeronautics and Space Administration
Goddard Space Flight Center
Greenbelt, Maryland 20771

Smithsonian Institution
Astrophysical Observatory
Cambridge, Massachusetts 02138

The Smithsonian Astrophysical Observatory
is a member of the
Harvard-Smithsonian Center for Astrophysics

The NASA Technical Officer for this grant is Dr. Robert Petre, Code 666, Laboratory for High Energy Astrophysics, Space Science Directorate, Goddard Space Flight Center, Greenbelt, Maryland 20771.

Harvard-Smithsonian
Center for Astrophysics

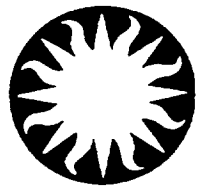

Preprint Series

No. 4314
(Received May 6, 1996)

ROSAT OBSERVATIONS OF TWO SOUTHERN SUPERNOVA REMNANTS

F.D. Seward
Harvard-Smithsonian Center for Astrophysics

K.E. Kearns
Harvard-Smithsonian Center for Astrophysics
and
Wesleyan University

and

K.L. Rhode
Wesleyan University

To appear in
The Astrophysical Journal

HARVARD COLLEGE OBSERVATORY SMITHSONIAN ASTROPHYSICAL OBSERVATORY
60 Garden Street, Cambridge, Massachusetts 02138

Center for Astrophysics
Preprint Series No. 4314

ROSAT OBSERVATIONS OF TWO SOUTHERN SUPERNOVA REMNANTS

F.D. Seward
Harvard-Smithsonian Center for Astrophysics

K.E. Kearns
Harvard-Smithsonian Center for Astrophysics
and
Wesleyan University

and

K.L. Rhode
Wesleyan University

ROSAT Observations of Two Southern Supernova Remnants

F. D. Seward[1], K. E. Kearns[1,2], K. L. Rhode[2]
[1]Harvard-Smithsonian Center for Astrophysics, Cambridge, MA, USA
[2]Wesleyan University, Middletown, CT, USA

ABSTRACT

The supernova remnants G327.1-1.1 and G327.4+0.4 (Kes 27) are located 1.5° apart in the constellation Norma. In 1980, Einstein IPC observations discovered that both were irregular filled-center X-ray sources with possible point sources superposed. This paper describes new ROSAT PSPC observations which both map the diffuse structure and clearly show several unresolved sources in each field. Both remnants have bright emitting regions inside the limb which might indicate the presence of high energy electrons accelerated by a pulsar. The interior region is more prominent in G327.1-1.1 than in Kes 27.

The spectra are relatively strongly absorbed, as expected from distant remnants close to the galactic plane. Comparison of the X-ray and radio maps of each remnant allows us to attribute some emission to a shell and some to the interior. With this information, a blast-wave model is used to derive approximate ages and energy release. Indications are that the Kes 27 supernova deposited $\sim 10^{51}$ ergs in the surrounding medium. The G327.1-1.1 event probably deposited a factor of 3-10 less.

Subject headings: supernova remnants, Kes27, G327.4+0.4, G327.1-1.1, ROSAT

1. Introduction

X-rays from both G327.1-1.1 and G327.4+0.4 (Kes 27) were first mapped by Lamb and Markert (1981) while using the *Einstein* IPC (a position-sensitive proportional counter) to search for counterparts to CosB γ-ray sources. Kes 27 was the brighter of the two by a factor of 4. X-rays were observed to originate most strongly from the interior of the remnant, and there was a knot of emission close to the northern limb which Lamb and Markert interpreted as an unresolved, perhaps compact, source. No *Einstein* HRI (a high-resolution channel-plate imager) observation was done. Radio maps are given by Caswell *et al*, (1975) and by Milne *et al* (1989). The size of the remnant is 16′ by 18′. Most of the radio emission comes from the limb which is bright in the east, faint in the north and west, and absent in the south. There is also an interior emission maximum with size about 2′ by 5′ and displaced 2′ from the center of the remnant. In their paper on SNR classification Kesteven and Caswell (1987) list Kes 27 as "difficult to classify".

G327.1-1.1 is 1.5° southeast of Kes 27. The structure in radio (Caswell, *et al*, 1975) appears to be a faint shell about 14′ in diameter but much of the remnant is obscured by a bright internal (or superposed) radio source. The x-ray data (Lamb and Markert, 1981) indicated an amorphous elongated shape of about 8′ extent close to the northern boundary of the remnant. There was also some evidence (Seward, 1990) that the remnant was detected by the *Einstein* HRI. The bright radio source was not evident in the *Einstein* data.

2. ROSAT Observations

The ROSAT PSPC (a position-sensitive proportional counter covering the band 0.1-2.4 keV) was used to observe Kes 27 from 9 to 14 March 1993 for a total ("livetime") of 13237 s. G327.1-1.1 was observed between 3 and 13 March 1993, for a total of 10516 s. In addition, a 2508 s ROSAT HRI observation of Kes27 was obtained on 15 September 1994.

The PSPC data were first screened to exclude periods of high background, shortening the Kes 27 effective exposure to 11940 s and that of G327.1-1.1 to 10087 s. Thus we rejected 10% and 4% of the data to eliminate periods when the detector was in a high flux of charged particles or scattered solar X-rays. To further enhance signal to noise for the remnants, data were restricted to the energy range 0.7 to 2.2 keV. Since low energy X-rays from these SNR are absorbed in the ISM, the low-energy data can be excluded from the morphological analysis. Any events with energy ¡ 0.7 keV are background or from foreground objects.

To map the X-ray emission, the centers of the fields containing the remnants were first extracted and corrected for vignetting. The stronger unresolved sources within the boundaries of the remnants were then subtracted and the resulting image smoothed to clearly show faint diffuse emission. Results are shown in Figs 1 and 4 which give X-ray structure of the two remnants. The unresolved sources are shown in Figs 2 and 5, which were smoothed with a finer spatial filter so point sources show clearly.

Figures 3 and 6 compare the ROSAT observations with radio data (Clark et al 1975, Milne et al 1989). The superposition of radio and X-ray maps provides a measure of the shape and extent of the remnants.

3. Morphology of Kes 27

The brightest X-ray emission from Kes 27 is from a region east of center, but emission from a well-defined eastern shell is nearly as bright . About 15% of the emission comes from the central region and the rest from the shell and interior of the remnant. The radio image defines a shell to the east, north and west. The brightest radio emission coincides with the X-ray bright eastern shell. X-rays are not observed from the northern radio shell.

Table 1 lists unresolved sources close in projection to Kes 27. None are yet identified with corresponding objects at other wavelengths. There are four unresolved sources superposed on the remnant itself. The brightest two, close to the northern limb, each have a soft component, which means that they are foreground objects and not associated with the remnant. Indeed, source #5 shows very little absorption and must be appreciably nearer to Earth than is Kes 27. The "northern source" found in the Einstein data by Lamb and Markert (1981) was a combination of these two objects. Source #2, at the center of the remnant is weak and at the limit of detection. It too shows some soft emission and is probably not associated with the remnant. Only source #4 is absorbed as strongly as the diffuse emission from Kes 27 and thus might lie at a similar distance.

#	RA (J2000)	dec (J2000)	PSPC ct s^{-1}	spectrum
1	15:47:09.1	-53:35:45	0.003	
2	15:48:31.8	-53:46:17	0.015	some soft emission
3	15:48:33.2	-53:39:13	0.025	some soft emission
4	15:48:38.5	-53:49:48	0.005	
5	15:48:41.1	-53:40:34	0.022	soft
6	15:49:39.8	-53:36:28	0.004	

Table 1: Unresolved X-ray sources close to Kes 27.

The three sources detected by the short HRI observation are listed in table 2. These were all detected by the PSPC but the HRI locations should be more accurate. Uncertainty in the locations of #3 and #5 is systematic and $\approx 5''$. Source #2 is weak and embedded in a strong background and counting statistics increase the the location uncertainty to $\approx 10''$.

#	RA (J2000)	dec (J2000)	HRI ct s^{-1}
2	15:48:29.0	-53:46:24	0.002
3	15:48:32.0	-53:39:08	0.009
5	15:48:39.9	-53:40:34	0.004

Table 2: X-ray sources in the HRI observation of Kes 27.

4. Morphology of G327.1-1.1

The brightest emission from G327.1-1.1 is from an extended region north of center but not at the northern edge of the remnant. X-ray and radio emission together define a shell in the south and southwest. No shell emission is observed from the northern boundary and the eastern edge is obscurred in the radio by a bright unresolved source. This radio source is not well correlated with structure of the x-ray remnant, but appears to be associated with a faint x-ray point source off-center but still within the boundary. 40% of the X-ray counts come from the bright "central" region. The spectrum of this region is definitely harder than that of the "shell" in the south, a southern extension, not detected by *Einstein*, but seen clearly in the PSPC data. The fainter radio contours and the X-ray emission define the boundary of the remnant.

Table 3 lists nearby unresolved X-ray sources, including three unresolved sources within the boundary. #1 lies just beyond the western boundary of Fig. 4-6, is unidentified, and is included here because it is relatively bright. #2 is at the position of a radio source listed by Griffith and Wright (1993). #3 is a 9th magnitude B star. #4 is absorbed enough to be associated with the remnant but has a softer spectrum than the remnant. #5 is weak and at the threshold of detectability. The position makes it a candidate for the counterpart of the bright unresolved radio source. #6 is quite soft and must be a foreground object. There are also other sources within the 2° PSPC field.

#	RA (J2000)	dec (J2000)	PSPC ct s^{-1}	spectrum	ID
1	15:52:26.3	-55:00:36	0.019	soft,far	
2	15:53:21.8	-55:15:47	0.007		PMN 1553-5515
3	15:54:22.2	-55:19:45	0.015		HD141926 (SAO243098)
4	15:54:43.2	-55:03:49	0.006	soft,far	
5	15:54:58.4	-55:06:00	0.005		strong radio source
6	15:55:10.4	-55:08:19	0.008	soft,near	

Table 3: Unresolved X-ray sources close to G327.1-1.1.

5. Spectral analysis

After background subtraction and removal of bright sources, PSPC spectra from both remnants were fit with simple models using the PROS and XSPEC software. These are not bright sources and the number of counts collected do not permit a precise derivation of spectral parameters. Clearly the spectra of both remnants are strongly absorbed in the ISM since, after background subtraction, no photons with energies less than 0.6 keV were detected.

We first searched for a difference in spectra between the central regions and the shells of

the remnants. Figure 7 compares spectra from the interior and the rim of each remnant. There is little difference between the spectrum of the central region (centered at $15^h48^m47^s, -53°46'$ and with diameter $6'$) and the east limb(centered at $15^h49^m18^s, -53°48.5'$ and with diameter $5'$) of Kes 27. Radiation from the interior of G327.1-1.1(centered at $15^h54^m28^s, -55°4.3'$ and with diameter $6'$), however, is clearly more energetic (harder) than that from the eastern rim (centered at $15^h54^m47^s, -55°10.5'$ and with diameter $6'$).

Model fitting to the Kes 27 data was done using all photons collected. The model was a single-temperature Raymond-Smith thermal model. (An optically-thin plasma with solar abundances, radiating primarily thermal bremsstrahlung and characteristic emission lines). The data do not warrant the use of more elaborate models. Figure 8 shows 90% confidence contours for the Kes 27 spectral fit.

Because the absorbing column and the temperature are strongly coupled in the thermal-model analysis, a range of solutions are equally acceptable to the PSPC data alone. A high temperature and low column will fit as well as a low temperature and a high column. We have used the *Einstein* MPC (a mechanically-collimated proportional counter sensitive in the 2-10 keV band) observations to remove this ambiguity. The quantity used was the ratio of MPC to PSPC count rates. The *Einstein* MPC rates were corrected for collimator transmission and the presence of other sources in the fields, assuming that the spectra of the unresolved sources were the same as that of the remnant. The observed PSPC sources were used to make this correction, which was $\approx$ 10%. The result indicates a temperature of kT = 3.2 $\pm$ 1.5 keV. There is, however, some danger in the use of this process. There could be higher energy emission from the "galactic ridge" which is not detected in the PSPC but increases the MPC rate. With this caveat, (the MPC/PSPC ratio used is, at worst, an upper limit), the result is shown in Figure 8 and listed in Table 4.

G327.1-1.1 is only half as bright as Kes 27, but $\approx$ 40% of the emission comes from the bright interior region. The interior emission is observably harder than that from the limb. We analysed the spectra of the center and of the limb separately. Each region contained only 1/5 as many counts as the Kes 27 spectrum and uncertainties in spectral parameters are consequently larger than those of the Kes 27 analysis. We have assumed that radiation from the center is nonthermal and that from the remainder is thermal. This is not required by the data. Figure 9 shows the result of a power law fit to the spectrum of the central region only. Both PSPC and MPC/PSPC results are shown. The correction for nearby sources to the MPC rate was $\approx$ 20%. The assumption here is that the MPC sees the central region to be much brighter than the rest of the remnant (and than the galactic ridge). The result shows that a Crab-like spectrum is compatible with the data but the parameters are not at all well determined.

Table 4 lists the spectral parameters derived from model fits to the Kes 27 and G327.1-1.1 spectra. For reasons given in section 8, the distance to Kes 27 is taken as 6.5 kpc. We use the same distance for G327.1-1.1 although the uncertainty is greater.

remnant	Kes 27			G327.1-1.1		
region	center	shell	whole	center	shell	whole
distance (kpc)	(6.5)		(6.5)	(6.5)		(6.5)
PSPC rate (s^{-1})	0.04±.01	4×0.062	0.23±.01	0.04±.01	5×0.018	0.11±.01
MPC rate (s^{-1})	-	-	1.10±.22	-	-	0.74±.14
(corrected)						
spectral model	power law	Raymond	Raymond	power law	Raymond	-
energy index	(1.0)	-	-	(1.0)	-	-
kT (keV)	-	3.2	3.2±1.5	-	0.8 ± .3	-
N_H (cm^{-2})	(1.3×10^{22})	-	$1.3 \pm .3 \times 10^{22}$	$(1.3\ times 10^{22})$	$1.3 \pm .4 \times 10^{22}$	-
L_x (0.2-2.4 keV)	3.6×10^{34}		1.5×10^{35}	3.6×10^{34}		1.5×10^{35}
(ergs s^{-1})						

Table 4: Spectral parameters, derived and (assumed), used in the analysis. Shell PSPC rates are explained in section 8.2. Figures 8-11 show uncertainties in more detail.

6. Non-thermal emission?

Both remnants were observed to investigate the possibility that the interior emission was synchrotron radiation powered by the spindown of an isolated neutron star. The internal region of G327.1-1.1, brighter and with more energetic X-rays than the shell of the remnant, is certainly suggestive of this. Fig 9 shows the result of a power law fit to the spectrum of this region and demonstrates that a Crab-like spectrum is compatible with (but not necessary to fit) the data. Assuming that the radiation is indeed non-thermal with a Crab-like spectrum, we derive an X-ray luminosity of 3×10^{34} ergs s^{-1} (table 4). This is 600 times less luminous than the Crab Nebula and, if a pulsar is present, its rate of loss of rotational energy is $\approx$ 70 times less than that of the Crab Pulsar (Seward and Wang, 1988).

Figures 3 and 6 show that neither interior region is a bright radio source, although there is some emission from the central part of Kes 27. This does not contradict the above discussion. If the X-rays, which are weak, are non-thermal the expected radio surface brightness is low. Observations of MSH 15-52 (Seward et al, 1984) illustrate exactly this situation, an X-ray synchrotron nebula with no observable radio counterpart.

7. G328.0+0.3

This remnant, cataloged by Green (1991), has a rather uncertain radio diameter of $\approx 6'$ and is located well within but $\approx 45'$ off-axis in the Kes 27 ROSAT field. There is no visible emission

above background at this location. There are two X-ray sources within $\approx 10'$ of this position, identified with the stars HD141646 (8th mag. G8III) and HD141945 (7th mag. F2IV). In this part of the PSPC field, stellar images are $\approx 6'$ in diameter and the HD141646 image overlaps the assumed edge of the remnant. Assuming uniform emission from the remnant, a 3 σ upper limit of 0.005 counts s^{-1} can be set on the count rate in the energy band 0.5-2.4 keV. If this object is indeed a supernova remnant, lack of detection implies low-temperature emission and absorption in the ISM. Soft emission implies that the remnant is not young and so the small diameter implies a distance well over 10 kpc. This is speculation. There is very little data.

8. Discussion

8.1. Distance

The bright remnant RCW 103 is located 5° from Kes 27 and has a kinematic HI distance of 3.3 kpc. Since the measured X-ray absorbing column density of Kes 27 is about twice that measured for RCW 103 (Nugent et al, 1984), we have assigned a distance of 6.5 kpc to this remnant. Although simple minded, this is not a bad approximation and there are no other reasonable distance estimates available. The spectra of the two regions of G327.1-1.1 do not yield a clear value of N_H. Because the low-energy cutoffs of the spectra are about the same as for Kes 27, we assign it the same distance.

To illustrate uncertainties, we take the distance in kpc to be 0.5 times the measured value of N_H in units of 10^{21} atoms cm^{-2}. Thus, the observed uncertainties in measurements of N_H translate to uncertainties in distances and parameters of the blast wave models can be plotted on the same graphs as the uncertainties in spectral parameters. The constant of proportionality is equivalent to an average ISM density (in the line of sight) of 0.65 atoms cm^{-3}.

8.2. Blast-wave model

Some insight can be obtained through application of a simple blast wave model (Sedov, 1959; Cox, 1972) as used, for example, by Rappaport et al (1974). The explosion is assumed to deposit energy E_0 into a uniform interstellar medium of density, n_0 atoms cm^{-3} ($n_H + n_{He} + n_C + ...$). Interstellar material is compressed by a factor of four and swept into a shell which (to conserve mass) has a thickness 1/12 the radius, R, of the remnant. Density within the shell is $n = 4n_0$. Material in the expanding shell has temperature, T, and is hot enough to emit X-rays. If the shell radius and temperature are known, the model gives the remnant age, t, and E_0/n_0.

$$(t/10^4 yr) = 1.60 \times 10^{-3}(T/keV)^{-0.5}(R/pc)$$

$$(E_0/10^{51} erg) = 1.16 \times 10^{-3}(n_0/atoms\ cm^{-3})(T/keV)(R/pc)^3$$

The density of the emitting plasma can be calculated from the measured X-ray luminosity of the shell, L_x, and the X-ray cooling function, $P(T)$, assuming an isothermal plasma with standard cosmic abundances.

$$L_x = 4\pi D^2 \eta C \approx n^2 V P(T).$$

Where V is the emitting volume, D is the distance, C is the PSPC count rate, and $\eta(T, N_H)$ is the PSPC calibration constant. η is the energy flux, leaving the source, which produces one count in the detector. Absorption is folded into the value of η so it is strongly dependent on T, N_H, and energy band.

The Sedov model was first applied to supernova remnants using observations of "average" parameters - a radius from low-resolution radio observations and an X-ray temperature measured with non-imaging detectors. Since the derived ages and energy releases were reasonable or, at least, did not disagree with conventional ideas, the model was acceptable. Modern imaging detectors, however, reveal structure in remnants which indicates that we are not observing a symmetrical explosion in a uniform medium. Still, there is surprising circular symmetry in the outermost part of many remnants, and other evidence for the presence of an outer shock.

To retain the model one assumes a circumstellar medium with embedded clouds and perhaps with density changes in the medium due to the history of the varying stellar wind of the progenitor star. The shock thus propagates outward in the circumstellar medium, heating the embedded clouds enough so they radiate strongly and perhaps evaporate. Large asymmetries have, in some cases, been shown to be caused by large molecular clouds (Petre et al, 1988, Tatematsu, 1988)

To apply this model to the two remnants under discussion, we have measured properties in sectors where the X-ray shell seems clearly, or best delineated. As indicated in Table 4, this encompasses only 1/4 of the shell of Kes 27 and 1/5 of the shell of G327.1-1.1. We then assume a complete shell with these characteristics and calculate the blast wave parameters. The blatant fact that the greater parts of both shells are not visible is attributed to inhomogeneities in the ISM which, through increased absorption, decreased density, decreased temperature, or some combination of these, renders parts of the shells invisible.

There is additionally, almost certainly, an unresolved small-scale clumpiness which will affect the result. Under these circumstances, the accuracy of the Sedov analysis is unknown. An analysis of Kes 79, however, did show that the calculation of E_0 was in agreement ($\pm 50\%$) with estimates of the thermal energy in the plasma (Seward and Velusamy, 1995). We speculate that the accuracy of the model will be well assessed in the future with the discovery of pulsars associated with a few "middle-aged" remnants, giving an independent measure of the age.

Results are given in Table 5 which lists the best-fit blastwave-analysis parameters derived for the two remnants. Because the remnants are not bright, there are large uncertainties. These are difficult to express succinctly so we follow the example set by Rappaport et al (1974) and use a graphical presentation. Since the uncertainty in distance appears directly in the radius and volume of the remnant and since we assume that the measured N_H is proportional to distance, we can write D, R, and V in terms of N_H. The calculated values of t, n_0, and E_0 can now be plotted on the graphs showing measured N_H and T and this has been done in Figures 10 and 11.

remnant	Kes 27	G327.1-1.1
diameter (′)	17	14
distance (kpc)	6.5	6.5
R (pc)	16.0	13.2
T (kev)	3.0	~ 0.8
n_0 (electrons cm^{-3})	0.095	~ 0.065
E_0 (10^{51} ergs)	1.1	~ 0.13
age (years)	3500	~ 7000

Table 5: Best blast-wave model parameters. E_0 and age are highly uncertain. See text discussion and figures 10 and 11 for details

Note that since the radius R is directly proportional to N_H, the lines of constant age show the expected dependence on R and T. n_0, however, varies little over the allowed range of N_H and T above 1 keV. The expected $D^{-0.5}$ dependence is somewhat balanced by the variation of $\eta(T, N_H)$ in this range. Also, at the higher temperatures, lines of constant E_0 track the acceptable range of N_H vs T. The N_H-T confidence contours fortuitously have the same slope in this region. Note that as one progresses to the lowest allowed temperatures, there is a considerable increase in the derived values of n_0, E_0, and t. There is, of course, a possible systematic error in the relationship between distance and N_H which does not appear in Figures 10 and 11. If our proportionality were off by 50%, the theoretical curves should be shifted up or down 50% with respect to the N_H scales.

The best-fit values of n_0 are low. Analysis of the emission from the Cygnus Loop, for example, yields a value of $n_0 = 0.25$ (Rappaport et al, 1974). Also the measured absorption in the ISM implies a much larger average density. Because the remnants are faint, the low value for n_0 is an inevitable result of the analysis. If the material were clumped, rather than the uniform distribution assumed within the shells, the density of emitting material would be greater.

As can be inferred from figures 10 and 11, n_0 can be increased by moving the remnants to lower temperatures (and larger distance). In this case the MPC data must be presumed contaminated by the galactic ridge and ignored. Low-temperature solutions permitted by the PSPC data alone would place the distances at 10-15 kpc, N_H at 2-3 $\times 10^{22}$ atoms cm^{-2}, the temperatures at 0.2-0.3 keV, and n_0 at ≈ 0.4 atoms cm^2. Kes 27 would have $E_0 \approx 4 \times 10^{51}$ ergs and age $\approx$ 23,000 years and G327.1-1.1, $E_0 \approx 0.8 \times 10^{51}$ ergs and age $\approx$ 17,000 years. Parameters

are now canonical for G327.1-1.1 but E_0 for Kes 27 is large. ASCA observations could eventually lead to a more precise derivation of these blast wave parameters.

9. Conclusions

For both remnants, the ROSAT-measured X-ray morphology is a big improvement over that of *Einstein*. The observed absorption indicates that both remnants are at a distance of 3 -10 kpc. Kes 27 has a well defined shell in the east which allows the application of a blast wave model. A similar analysis is applied to G327.1-1.1 although the shell and spectrum are not nearly as well defined. The derived density of material in both remnants is low. If the remnants are at the same distance, the smaller size and lower temperature of G327.1-1.1 implies a lesser supernova energy release than that which produced Kes 27. This is not the case if G327.1-1.1 is farther away.

There is interior emission from both remnants. The harder spectrum of the interior emission of G327.1-1.1 might indicate synchrotron emission. That and the relative strength of the interior emission makes this a candidate for an older composite remnant.

This work was supported by NASA through contract NAS8-39073 and grant NAG5-1938. We thank J. Hughes, P. Slane, O. Vancura, and the Referee for useful discussions and for helpful comments on the manuscript.

REFERENCES

Caswell, J.L., Clark, D.H., Crawford, D.F., Green, A.J., 1975 *Aus. J. Phys. App. Supp.* 37, 39.

Clark, D.H., Caswell, J.L., Green, A.J., 1975 *Aus. J. Phys. App. Supp.* 37, 1.

Cox. D. 1972, *Ap.J.*, 178, 159.

Green, D.A. 1991, PASP, 103, 209.

Griffith, M.R. and Wright, A.E. 1993, *AJ* 105, 1666

Kesteven, M.J., and Caswell, J.L. 1987, *Astr. Ap.* 183, 118.

Lamb, R.C., Markert, T.H., 1981, *Ap.J.*, 244, 94.

Milne, D.K., Caswell, J.L., Kesteven, M.J., Haynes, R.F., and Roger, R.S. 1989, *Proc. Astron. Soc. Aus.* 8 (2), 187.

Rappaport, S., Doxey, R., Solinger, A. and Borken, R. 1974, *Ap.J.*, 194, 329.

Petre, R., Szymkowiak, A.E., Seward, F.D., and Willingale, R., 1988, *Ap.J.* 355, 215.

Seward, F.D., 1990, *Ap.J. Suppl.* 73, 781.

Seward, F.D., Harnden, H.R. Jr., Szymkowiak, A., and Swank, J. 1984, *Ap.J.* 73, 781.

Seward, F.D. and Velusamy, T. 1995, *Ap.J.*, 439, 715.

Sedov, L., 1959, *Similarity and Dimensional Methods in Mechanics*, New York, Academic Press, 334.

Tatematsu, K., 1988, PhD thesis, Nagoya University.

10. Figure Captions

Figure 1. Diffuse X-ray emission from Kes 27. PSPC data in the energy range 0.7 to 2.2 keV have been smoothed with a Gaussian filter with FWHM = 1.6′. Three unresolved sources (numbers 3, 4, and 5 in Fig. 2) have been removed to avoid distortion of the SNR diffuse emission. Peak diffuse surface brightness is 0.0025 counts arcmin^{-2} s^{-1} and the logarithmic contours are spaced a factor of 1.2. Coordinates are epoch 2000.

Figure 2. Unresolved sources in and around Kes 27. Data have been smoothed with a Gaussian filter with FWHM = 0.3.′ Sources are numbered as in Ta ble 1. Contours are taken from Fig. 1.

Figure 3. Radio and X-ray emission from Kes 27. Diffuse X-ray emission is shown by the same grey-scale used in Fig. 1. The radio map is from Milne et al (1 989). Faint radio contours are logarithmic and spaced a factor of 2. The two bri ghtest intervals are ∼ linear. Note that the eastern limb clearly emits both radio and X-rays and that the central X-ray emission feature does not coincide wi th the central radio feature (which is an emission maximum) although they do overl ap. No X-ray emission is observed from the western limb.

Figure 4. Diffuse X-ray emission from G327.1-1.1. PSPC data in the energy range 0.7 to 2.2 keV have been smoothed with a Gaussian filter with FWHM = 1.4′. Three unresolved sources (numbers 3, 4, and 6 in Fig. 5) have been removed to avoid distortion of the SNR diffuse emission. Peak diffuse surface brightness is 0.0026 counts arcmin^{-2} s^{-1} and the logarithmic contours are spaced a factor of 1.2. Coordinates are epoch 2000.

Figure 5. Unresolved sources in and around G327.1-1.1. Data have been smoo thed with a Gaussian filter with FWHM = 0.3′. Sources are numbered as i n Table 3. Source 5 is a possible counterpart of the bright unresolved radio sour ce shown in Fig. 6. Contours are taken from Fig. 4.

This preprint was prepared with the AAS LaTeX macros v3.0.

Figure 6. Radio and X-ray emission from G327.1-1.1. Diffuse X-ray emission is shown by the same grey-scale used in Fig. 4. Three point X-ray sources have b een removed. The radio map is from Clark et al (1975) and spacing of contours is linear. The resolution of the radio telescope is indicated in black. Note that s ome X-ray emission is observed from the southeastern limb and the brightest X-ray emission is from the interior of the remnant, close to the northern limb.

Figure 7. Comparison of pulse height spectra from the interior (filled points) and rim (open points) of each remnant showing that the interior spectrum of G327.1-1.1 is harder than that from the outer region. Rim spectra have been obtained only from regions where shell-like structure was seen and have been normalized (by total counts) to the interior. The vertical scale shows the number of counts/channel for the interior regions. The horizontal scale is logarithmic and ranges from 0.5 to 2.5 keV. Lines to guide the eye connect data points. Error bars show 1σ statistical uncertainties. The t wo spectra from Kes 27 are almost the same.

Figure 8. Allowed region for Raymond-Smith thermal model fit to spectrum of Kes 27. 90% confidence contours are shown for the PSPC fit and for the observed ratio of *Einstein* MPC rate to ROSAT PSPC rate. See text for details.

Figure 9. Allowed region for power law fit to spectrum of the inner part of G327.1-1.1. 90% confidence contours are shown for the PSPC fit and for the observ ed ratio of *Einstein* MPC rate to ROSAT PSPC rate. See text for details.

Figure 10. Blast-wave model parameters for Kes 27 overlaid on PSPC 90% con fidence contours from Fig. 7. The region which also fits the MPC data is indicate d. The parameters shown top to bottom are: age in years, ISM density in atoms cm^{-3}, and supernova energy release in units of 10^{51} ergs.

Figure 11. Blast-wave model parameters for G327.1-1.1 overlaid on PSPC 90% confidence contours for a thermal fit to the spectrum of the southern "shell". The parameters shown top to bottom are: age in years, ISM density in atoms cm^{-3}, and supernova energy release in units of 10^{51} ergs.

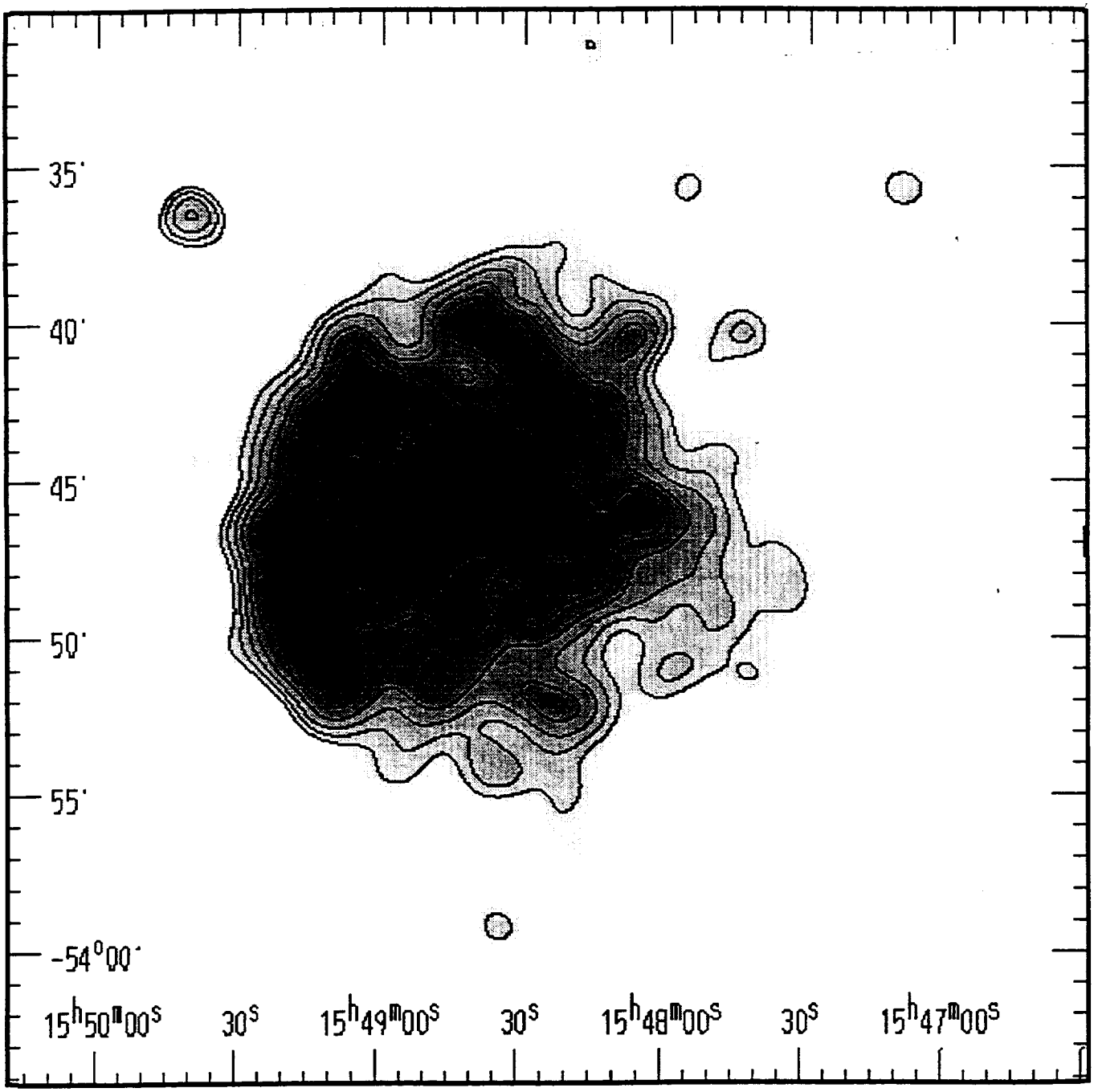

Figure 1.

Fig 1

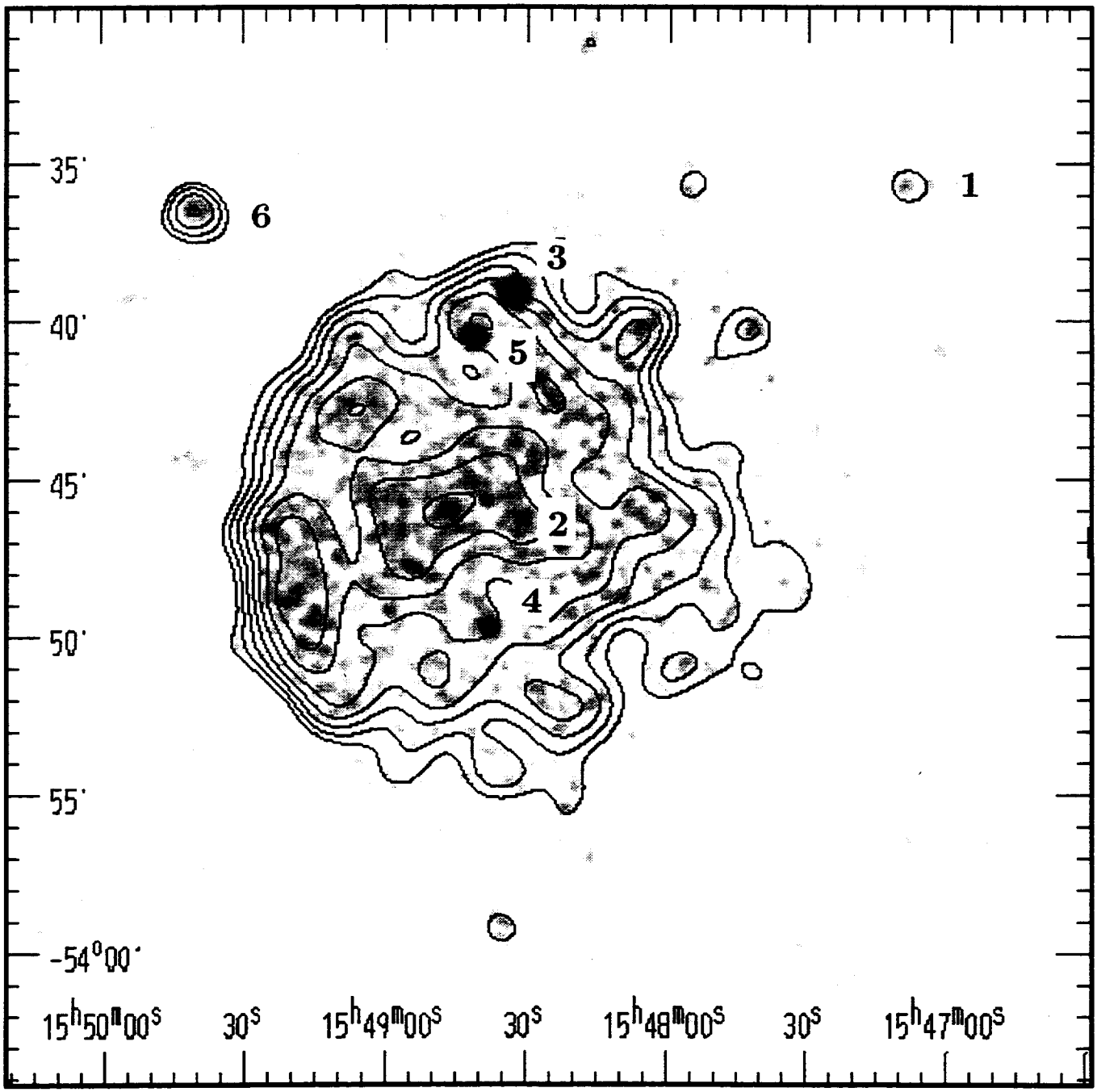

Figure 2.

Fig 2

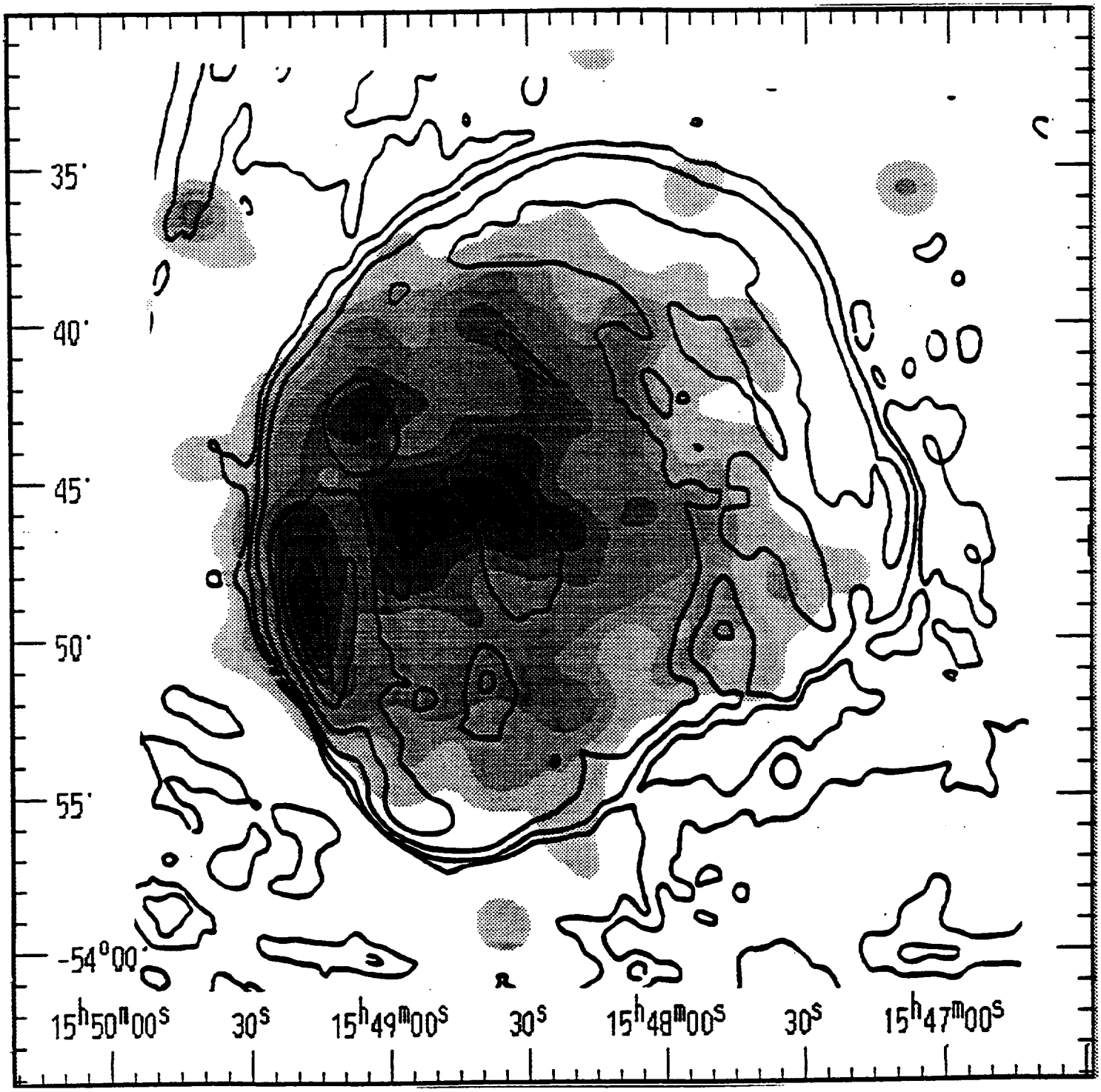

Figure 3.

Fig 3

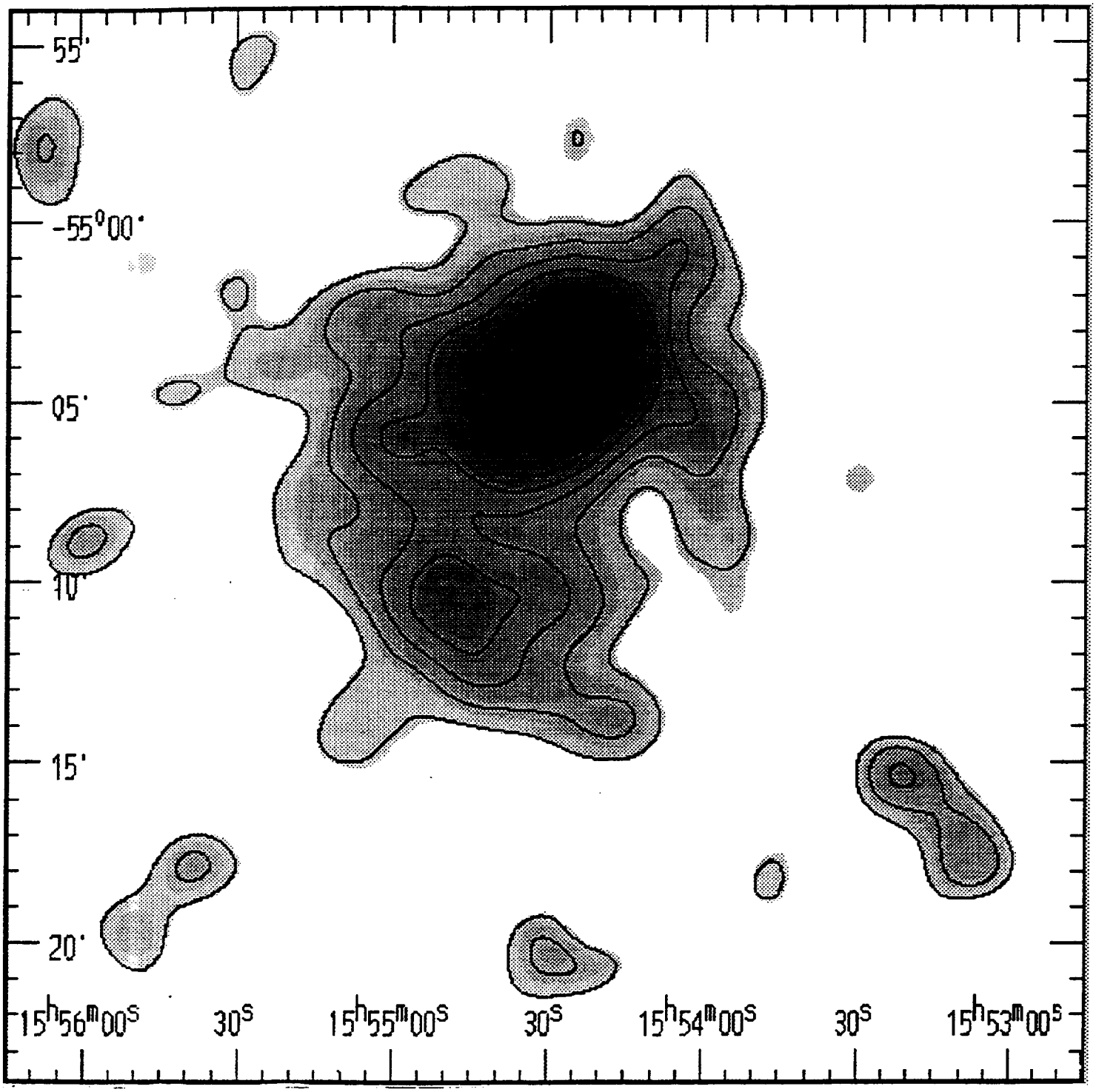

Figure 4.

Fig 4

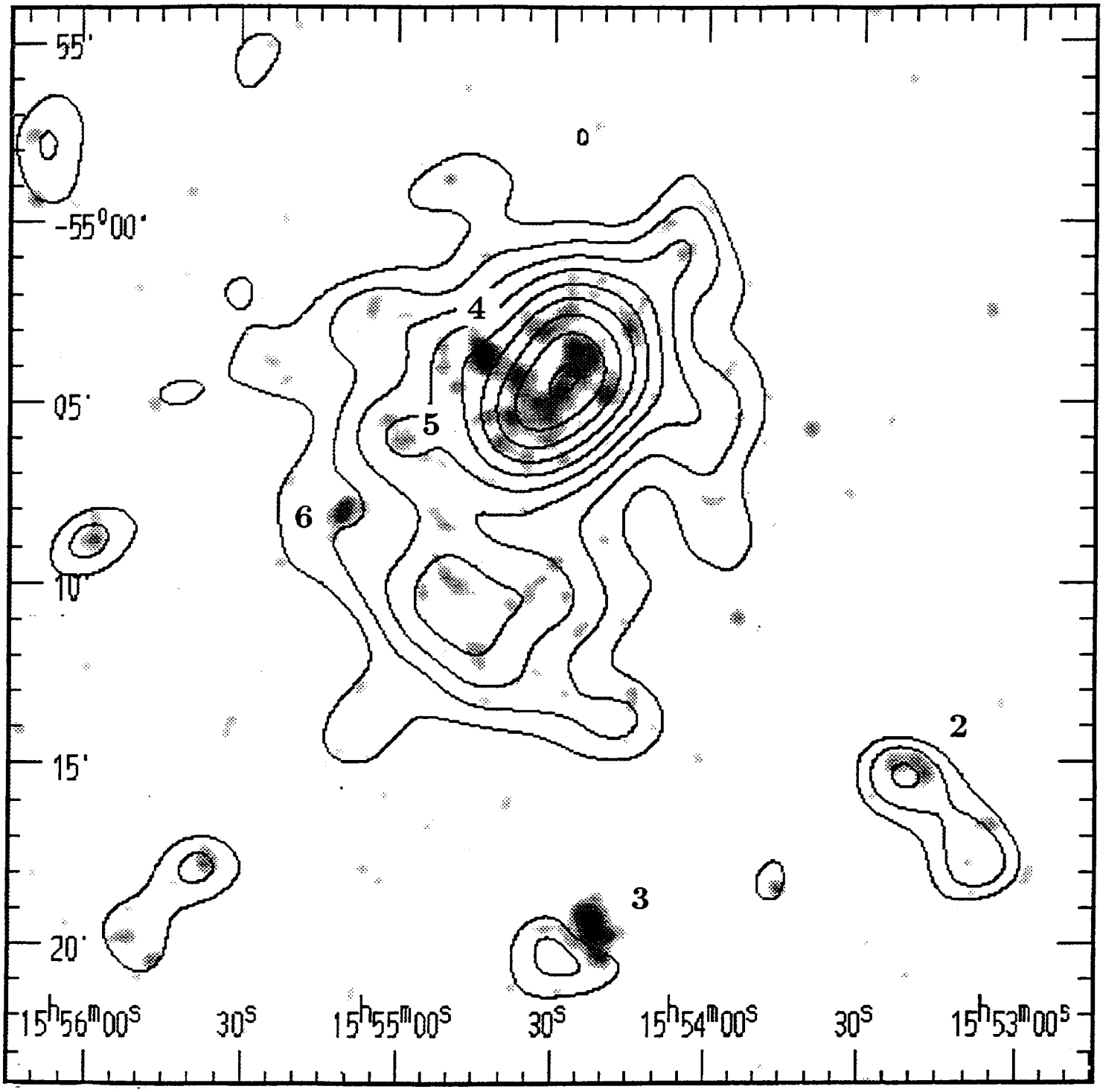

Figure 5.

Fig 5

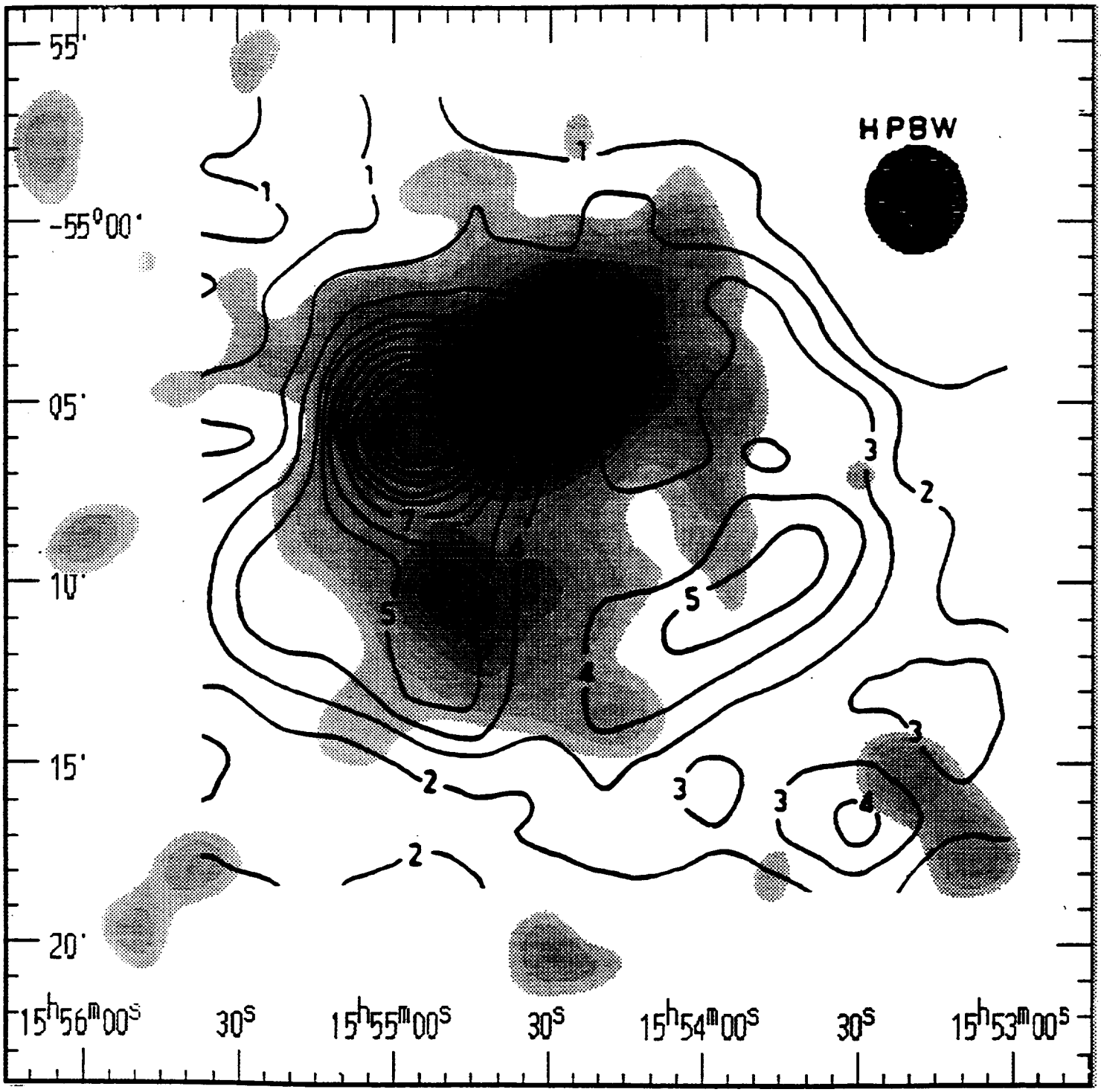

Figure 6.

Fig 6

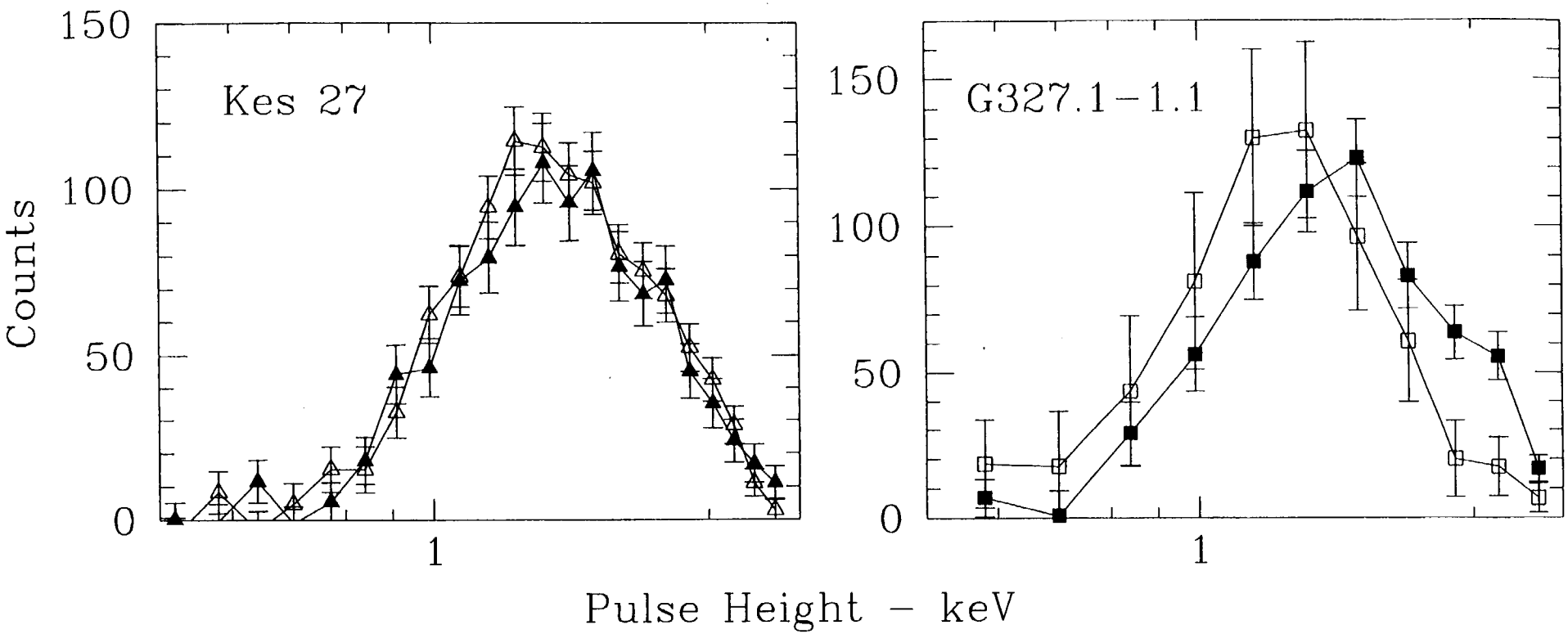

Figure 7.

Fig 7

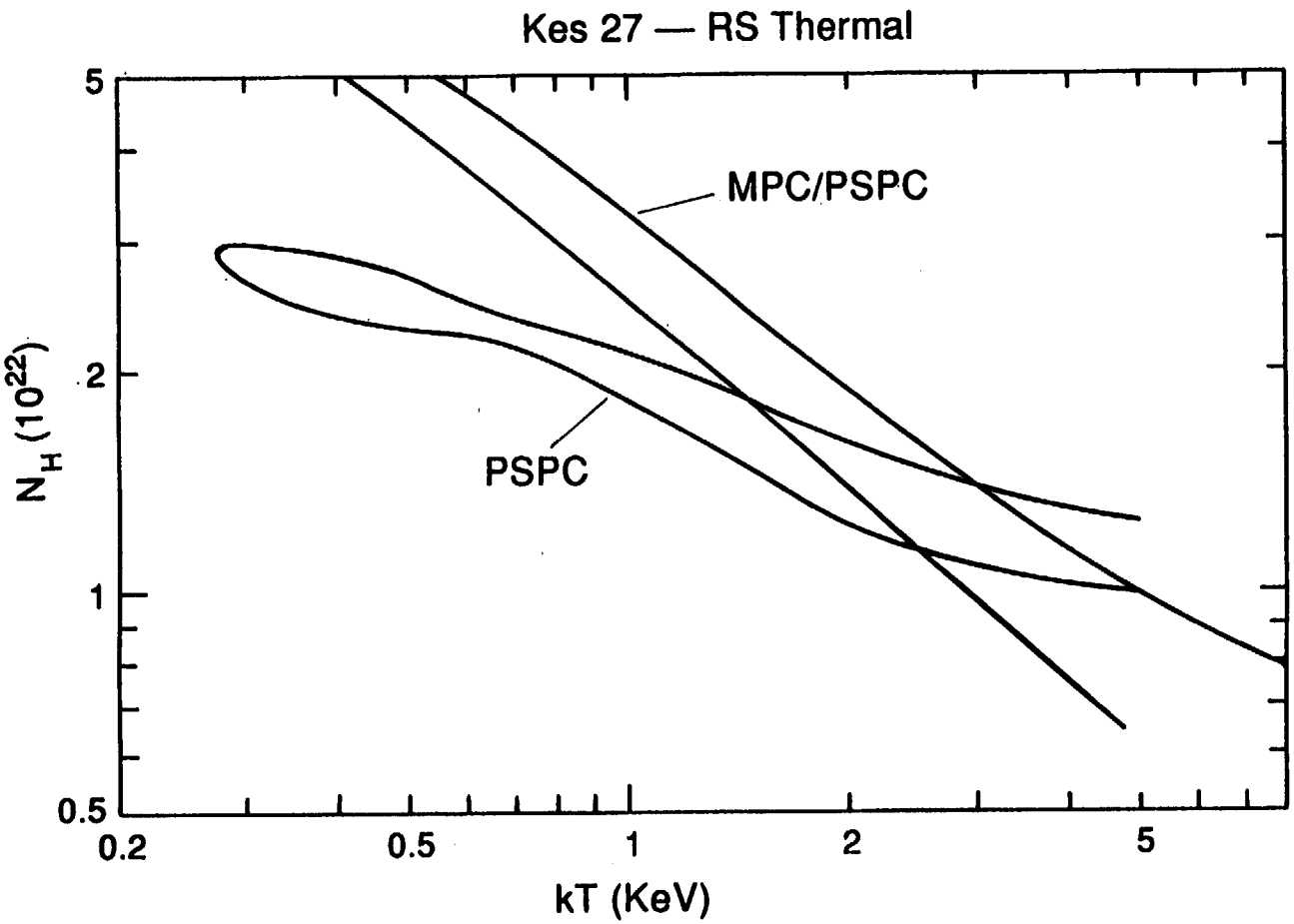

Figure 8.

Fig 8

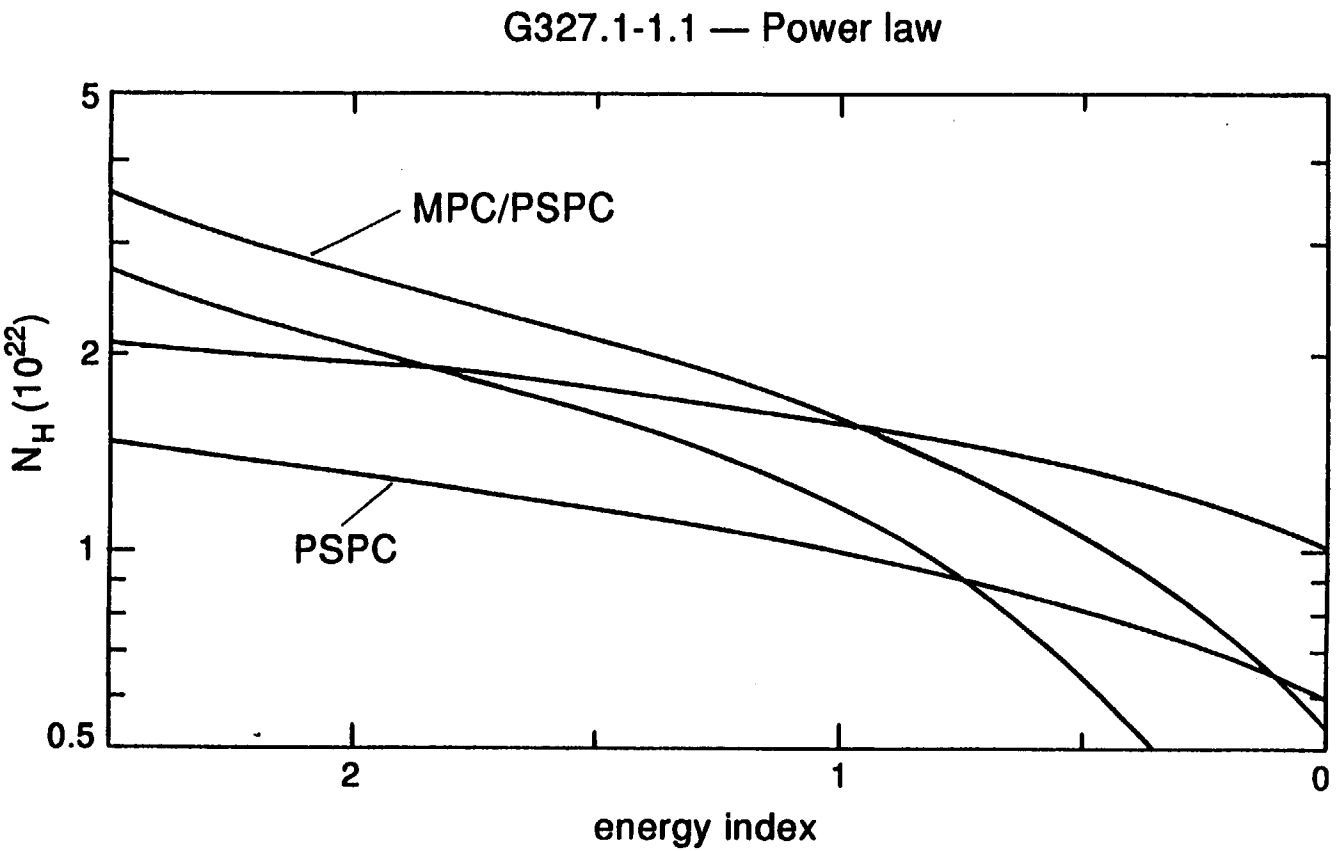

Figure 9.

Fig 9

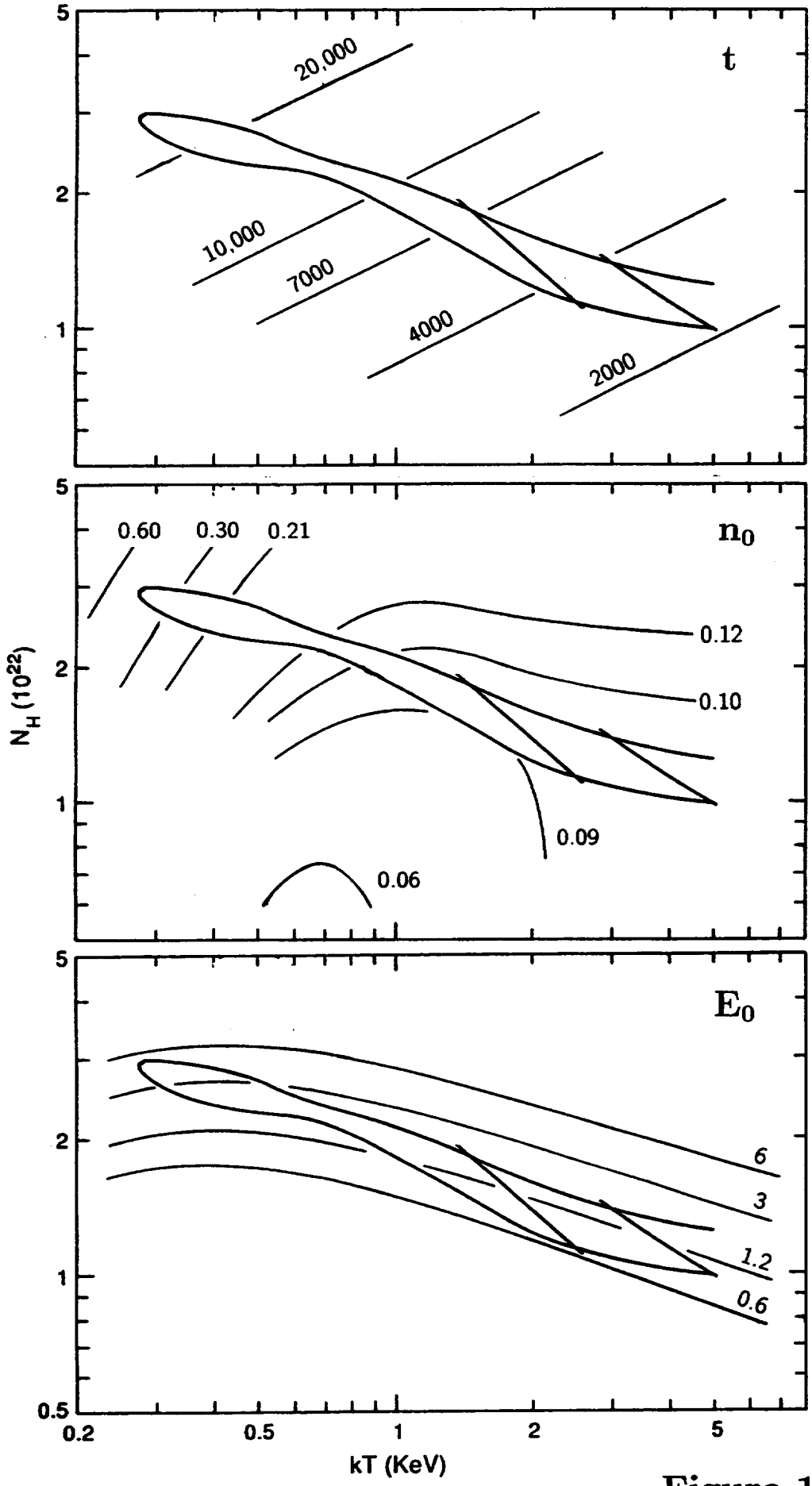

Figure 10.

Fig 10

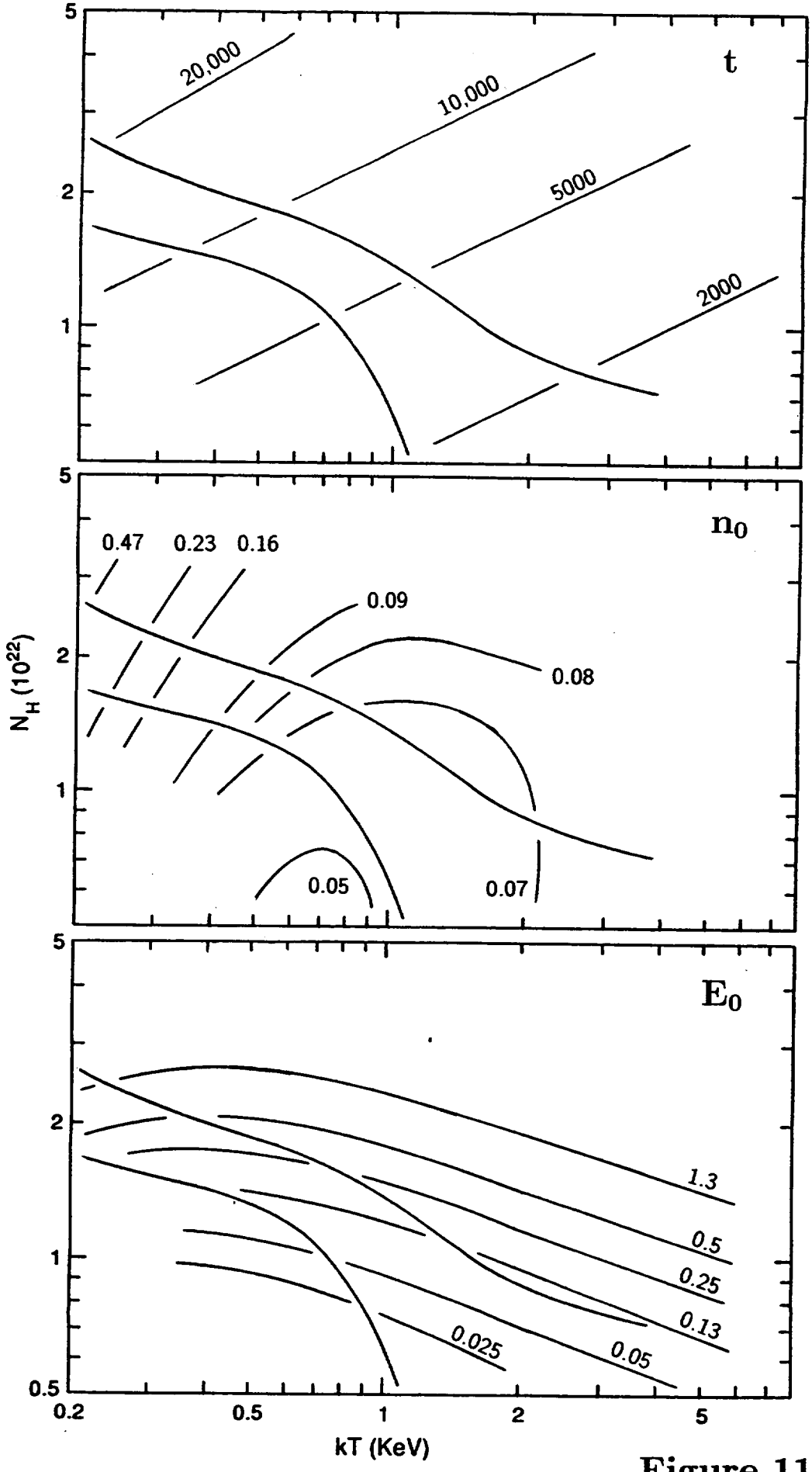

Figure 11.

Fig 11